# Fluorescence Anisotropy and Crystal Structure of Individual Semiconductor Nanocrystals†

**Felix Koberling,‡,§ Ute Kolb,‡ Günther Philipp,|| Inga Potapova,‡ Thomas Basché,‡ and Alf Mews*,‡**

*Institut für Physikalische Chemie, Universität Mainz, Mainz D-55099, Germany, and Max-Planck-Institut für Festkörperforschung, Heisenbergstrasse 1, Stuttgart D-70569, Germany*

*Received: December 22, 2002; In Final Form: April 16, 2003*

We investigate the polarization state of the fluorescence emission of individual CdSe/ZnS nanocrystals and try to establish a correlation with their crystallographic properties. The crystallinity and orientation of the particles are examined by transmission electron microscopy (TEM). These micrographs are compared with simulated TEM images. The polarization of the fluorescence light is investigated with a method in which the orientation of the transition dipole can be determined within seconds even though the fluorescence shows strong intensity fluctuations. The results show that even spherical particles emit elliptically polarized light, which can in principle be explained by a 2D transition dipole ("bright plane"). For a few particles, we could directly compare the polarization state with the crystallographic structure of the same nanocrystals. The findings reveal that a well-defined polarization state can even be observed for particles with stacking faults and polycrystalline nanocrystals.

## I. Introduction

The correlation of structural and electronic properties will develop into an important tool for the investigation of nanostructures, where small variations in size, shape, or orientation lead to large changes in the physical properties.[1,2] For example, CdSe semiconductor nanocrystals (NCs) in the size regime between 2 and 8 nm in diameter consist of 100−5000 CdSe units. The volume of a particle that is approximately 3 nm in diameter is increased by 100% when it is covered by one additional monolayer of CdSe. Because the electronic confinement in these nanocrystals is strongly size-dependent, large changes in the photophysical properties are observed. For instance, the fluorescence color of CdSe particles can be tuned over almost the entire visible range.[3]

The fluorescence quantum yield, however, is strongly dependent on the surface structure of the particles.[4] In general, colloidal semiconductor particles consist of an inorganic core and a shell of molecular ligands that can possibly donate or accept charge carriers. Therefore, the photogenerated electrons or holes can be transferred to the surface ligands, which leads to fluorescence quenching.[5] Also, it has been proposed that unsaturated surface atoms might act as traps for electrons and/or holes and influence the fluorescence quantum yield.[6] Therefore, several methods have been developed to cover the particles with inorganic material of a higher band gap.[7−9] It has been shown that the coverage of CdSe nanocrystals with a few monolayers of CdS[10] or ZnS[11] increases the quantum yield to more than 80%. The brightness and stability of the these core−shell particles might lead to many technological applications such as NC LEDs,[12−15] NC biolabels,[16,17] or even NC lasers,[18,19] the feasibility of which has already been demonstrated on a laboratory scale.

Although the color tunability of the NCs is the driving force for many applications, the underlying size dependence of the optical properties often hampers detailed fundamental research of the nanostructures. Even though the size distribution of these colloidal quantum dots can be narrowed down to less than 5%,[3] many features in the optical spectra are still smeared out because of the remaining sample inhomogeneities.[20] These inhomogeneities are caused not only by different particle sizes but also by variations in the shape, surface passivation, or crystallinity of the NCs.[21]

To overcome these problems, several microscopic techniques have been employed to explore the structural and electronic properties of individual nanocrystals. The most powerful method for structural analysis is high-resolution transmission electron microscopy (HRTEM), which allows one not only to determine the size of the particles but also to investigate their shape, crystal structure, and crystallographic alignment.[22,23] Moreover, even the chemical composition of single dots can be addressed with additional TEM tools such as electron energy loss spectroscopy (EELS).[24] The electronic level structure can be studied directly by electron transport measurements through single nanocrystals. This can be performed either in a lateral arrangement where the dots are bridging adjacent electrodes[25] or with the aid of a scanning tunneling microscope (STM) where the electrons tunnel from the tip through the dot into the substrate.[26]

The photophysics of single nanocrystals can be analyzed by fluorescence microscopy.[27] Since the application of this technique,[28,29] several interesting phenomena of nanoparticles that would have been difficult to infer from ensemble measurements were observed. Interestingly, it was found that the fluorescence of the nanocrystals fluctuates and can be interrupted by dark periods of many seconds. This fluorescence blinking behavior depends on experimental conditions such as the thickness of the passivating shell, the surrounding gas environment,[30,31] the excitation intensity,[28] and the temperature.[32] Due to the current model, fluctuations of charges in or around the particles are responsible for the fluorescence fluctuations.[28,33] It is assumed

† Part of the special issue "Arnim Henglein Festschrift".

* Corresponding author. E-mail: alf.mews@uni-mainz.de.

‡ Universität Mainz.

§ Present address: PicoQuant GmbH, Rudower Chaussee 29, 12489 Berlin, Germany.

|| Max-Planck-Institut für Festkörperforschung.

10.1021/jp027800b CCC: $25.00 
Published on Web 07/04/2003

that either the electron or the hole of a photoexcited NC is trapped at the surface, leaving a delocalized charge carrier inside the NC core.[34] This leads to the dark state of the particle because Auger quenching processes can happen in a charged dot (i.e., the quenching rate due to the excess charge is much faster than the fluorescence rate[35]). In fact, electrostatic force measurements of individual particles revealed that the net charge of single nanocrystals fluctuates in time.[36]

These temporal changes in the electronic properties might also be the reason for the multiexponential florescence decay time that has been observed for ensembles of colloidal nanoparticles.[37] For single emitters, the fluorescence decay curve was first determined by a so-called "photon antibunching experiment" where the time delay between consecutive emitted photons was measured.[38,39] These measurements revealed different but almost monoexponential decays between 12 and 28 ns for individual dots. With direct decay-time measurements using pulsed excitation and time-correlated single-photon counting (TCSPC), the fluorescence decay time of single dots could be directly compared with the fluorescence intensity.[40] It was shown that a long excited-state lifetime was correlated with a high fluorescence intensity, which was explained by a model where dynamic quenching processes lead to intensity fluctuations. Very recently, it was demonstrated that the fluorescence rate of single emitters can be strongly increased when the particles are close to a rough metal surface. This leads to a strong fluorescence enhancement because the fluorescence rate of particles that are close to the metal interface is higher than the Auger quenching rate in charged dots.[41]

The examples mentioned above show that the fluorescence properties of individual semiconductor nanocrystals are strongly influenced by environmental or surface effects. Of similar importance is the investigation of the effect of fluorescence behavior upon crystallographic characteristics (i.e., upon the shape, orientation, and crystallinity of the nanocrystal). The first experiments toward this goal revealed that the emitted fluorescence light of individual particles has an anisotropic polarization distribution.[42] The observed polarization state was explained by a 2D fluorescence transition dipole in almost spherical NCs, which was expected to lie perpendicular to the 001 crystallographic axis of ideal and randomly orientated nanocrystals.[43] However, measurements of the polarization state of CdSe nanorods, which are elongated along the 001 axis,[44] indicated that these particles emit linearly polarized light. The different behavior of nanocrystals and nanorods was explained theoretically by a length-dependent change of the electronic structure in NCs.[45] It is expected that the hole states, which are involved in the fluorescence transitions, are different for NC dots and NC rods. In particular, it was shown that a level crossing was calculated at an aspect ratio of about 1.3, which would explain the change from unpolarized to linearly polarized emission.[46]

However, all of these measurements and calculations assume "ideal" nanocrystals in terms of shape and crystallinity. In none of the experiments has the possibility or influence of lattice imperfections been taken into account. Therefore, in this paper, we attempt a detailed study of the crystal structure and fluorescence anisotropy of the same set of particles. We present a new type of fluorescence measurement that allows us to determine the fluorescence polarization state within a few seconds, even for particles with strong fluorescence blinking. Furthermore, we show HRTEM measurements that reveal that a high percentage of the particles are not single-domain crystals but comprise stacking faults of different degrees or are even polycrystalline. This is confirmed by TEM-image simulations that are based on ideal single crystals with different orientations relative to the substrate. Finally, we compare the fluorescence polarization data and the TEM images for a few identical individual nanocrystals.

## II. Experimental Section

The synthesis of CdSe/ZnS particles is based on standard methods[47] with slight modifications. Here we focused on the preparation of relatively large particles[48] with a high fluorescence quantum yield.[49] Trioctylphosphine oxide (TOPO), dodecylamine (DA), tributylphosphine (TBP), toluene, methanol, and hexamethyldisilathiane ($(TMS_2)S$) were purchased from Aldrich, dimethylcadmium ($CdMe_2$) and diethylzinc ($ZnEt_2$), from Strem Chemicals, and selenium powder, from Alfa. Toluene, methanol, and $CdMe_2$ were distilled before use, and $ZnEt_2$ was filtered. Octylphosphonic acid (OPA) was prepared according to ref 50. For the particle synthesis, stock solutions of 1.5:1 Cd/Se and 1:1 Zn/S were prepared in a glovebox and stored in sealed flasks in a refrigerator. The CdSe stock solution consisted of 0.197 g of Se and 0.534 g of $CdMe_2$ dissolved in 20 g of TBP. The ZnS stock solution was a mixture of 0.309 g of $ZnEt_2$ and 0.446 g of $(TMS)_2S$ in 20 g of TBP.

For the preparation of the CdSe particles, which was carried out under continuous argon flow, a mixture of 6,00 g of TOPO and 0.03 g of OPA was heated under vacuum for 1 h ($p = 3$ mbar, $T = 90$ °C). Then the temperature was raised to 360 °C, and 2 mL of the CdSe stock solution was quickly injected, followed by a dropwise addition of another 2.5 mL of the stock solution within the next 30 min. This reaction mixture was left stirring in an Ar flow at 260 °C for 24 h. After cooling to room temperature, 30 mL of methanol was added, leading to the precipitation of the particles, which were separated from the reaction solvent by centrifugation and redispersed in toluene.

For the ZnS coating, a mixture of 2.00 g of TOPO and 3.00 g of DA was heated at $p = 150$ mbar, $T = 90$ °C for 1 h. To this mixture, the toluene solution of CdSe was added, and the toluene was removed by distillation. Then a calculated amount of the ZnS stock solution (nominally for three monolayers of a ZnS shell) was added dropwise at 220 °C within 20 min under continuous Ar flow. The calculation of the amount of ZnS is based on the concentration of CdSe particles as estimated from optical measurements.[5] Then the temperature was decreased to 100 °C, and the reaction mixture was left stirring for an additional 3 h. After cooling to room temperature, 30 mL of methanol was added to precipitate the particles, which were redispersed in toluene after separation.

The absorption and fluorescence spectra of the CdSe/ZnS particles are shown in Figure 1a and b, respectively. For comparison, the fluorescence spectrum of the uncoated CdSe particles is also shown (Figure 1c). The fluorescence quantum yield of the uncoated particles is relatively small (0.5−1% as compared to that of a dye solution of R6G). This is most likely due to the synthesis procedure because it has already been shown that a longer reaction time will lead to a lower fluorescence quantum yield.[51] However, after overcoating the particles with nominally three monolayers of ZnS in a mixture of TOPO and DA as the solvent, the quantum yield is increased to more than 60%, and the fluorescence band is slightly red-shifted.[47]

For TEM measurements, a droplet of the colloidal NC solution was placed on a copper grid supported with a thin amorphous carbon film. The measurements were performed with a Tecnai F30ST (FEI) operated at 300 kV. All high-resolution electron micrographs were taken at the "Scherzer focus".

The substrate used for combined TEM and optical measurements is sketched in Figure 2. It consists of a 0.4-mm-thick

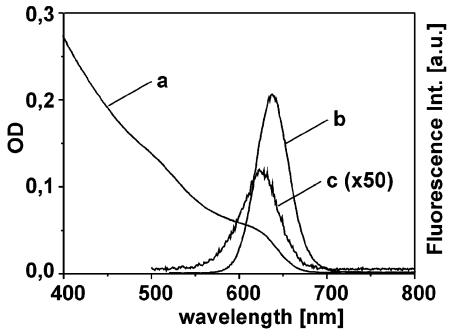


**Figure 1.** (a) Absorption and (b) emission spectra of the CdSe/ZnS core/shell particles in solution. (c) Fluorescence spectrum of the initial CdSe core particles. Although the fluorescence quantum yield of the core particles is very weak (<1%) because of the long reaction time (24 h), the quantum yield is increased to more than 60% after coverage with ZnS in a mixture of TOPO and DA.

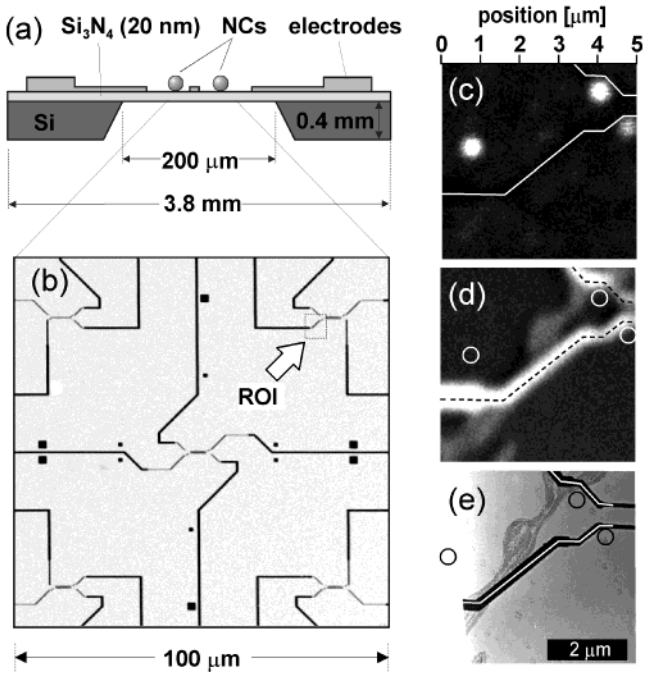


**Figure 2.** Localization of the same individual nanocrystals on a substrate with markers in the optical microscope and the TEM. (a) Cross section of the silicon substrate covered with an $Si_3N_4$ membrane, on which the nanocrystals are deposited. (b) Top view of the free-standing $Si_3N_4$ membrane in the center of the substrate, with the electrode structure that has been used as a marker. The square defines the region of interest (ROI). (c−e) Fluorescence, reflection, and TEM images, respectively, of the ROI marked in b. By overlaying the different types of images from the same substrate area, the position of the luminescing nanocrystals with respect to the markers can be specified.

silicon wafer covered with 20 nm of $Si_3N_4$ on which thin lithographically defined electrode structures are deposited. The electrode structures are usually used for electronic transport measurements,[52] but in our experiments, they served as markers to localize the same nanocrystals in the optical and electron microscope.[53] To perform TEM investigation, the back side of the substrate was etched away in the center region, leaving behind a free-standing $Si_3N_4$ membrane with an area of about $200 \times 200\ \mu m^2$, which can be seen in the optical micrograph of Figure 2b.

The confocal microscope for the optical measurements is based on a commercial inverted microscope (Zeiss, Axiovert 135 TV). For excitation, we used the 488-nm line of an Ar−Kr ion laser that was circularly polarized with a $\lambda/4$ wave plate. The typical excitation power was 70 nW, which results in an excitation intensity of 41 W/cm$^2$ in the center of the excitation focus of the microscope objective (100×, NA = 0.9). To avoid any drift during the measurements, the sample is mounted on an actively stabilized piezo scanner (PI, P-731.29) that can be moved over a range of $100 \times 100\ \mu m^2$ with an accuracy of less than 10 nm. For coarse approach, the whole piezo scanner including the sample can be moved over a range of ±10 mm using a manually driven translation stage equipped with differential micrometer screws. This option is needed to localize the region of interest (ROI) on the substrate. During coarse approach, the microscope is not operated in the confocal mode but in the wide-field mode (i.e., a wide-field illumination lens is placed in the excitation path, thus illuminating a sample area of several hundred $\mu m^2$, which can be viewed through the eyepiece of the inverted microscope. Once the ROI is localized, the microscope is switched back to the confocal mode, and an image is taken by raster scanning the sample stepwise through the focus of the microscope objective while collecting the fluorescence or scattered excitation light.

For example, if the ROI marked with a square in Figure 2b is scanned through the excitation focus and the scattered excitation light is absorbed by a long-pass optical filter (OG 590), then the fluorescence spots due to isolated nanocrystals can clearly be observed as shown in Figure 2c. The luminescing spots are far bigger than the nanocrystals because of the fundamental diffraction limit in far-field optics. Each single nanocrystal acts as a point light source and causes a Gaussian-shaped intensity profile in the fluorescence image with a fwhm of about 300 nm, which directly reflects the lateral resolution of the confocal microscope. If the long-pass filter is replaced, then the image is dominated by the backscattered excitation light, which is much stronger at the metallic electrodes as shown in Figure 2d. From the superposition of the two images, the position of the fluorescing nanocrystals with respect to the markers can be determined within an accuracy of <±200 nm. Figure 2e shows a low-resolution TEM image of the same ROI where the circles mark the areas of the fluorescing spots in which the nanocrystals are expected to reside.

For single-dot spectroscopy, a fluorescing spot is moved into the center of the excitation focus and the fluorescence light is guided to the detection units. The detection part of the microscope (Figure 5a) allows us to determine the polarization of the fluorescence light and to collect fluorescence spectra of individual emitters. To determine the degree of polarization, the fluorescence light is divided with a 50/50 beam splitter (BS) and guided to two separate single-photon counting modules (APD1 and 2). In front of APD1, we placed a linear polarizer rotating with a frequency of 0.83 Hz, and the signal at APD2 is used to record the fluorescence fluctuations only. For spectroscopy, the light can also be guided to a spectrograph equipped with a liquid-nitrogen-cooled CCD camera by changing the position of the flip mirror (FM).

## III. Structural Investigation

To explore the quality of the sample in terms of shape and crystallinity, we performed a detailed TEM study of the CdSe/ZnS particles deposited from a high-concentration solution on an amorphous carbon support.

The HRTEM image of Figure 3 shows an arbitrary section of the substrate where about 10 nanocrystals can be seen. Obviously, most of the particles are almost spherical or slightly elongated. This shape is expected because the nanocrystals were prepared with a relatively low precursor concentration over

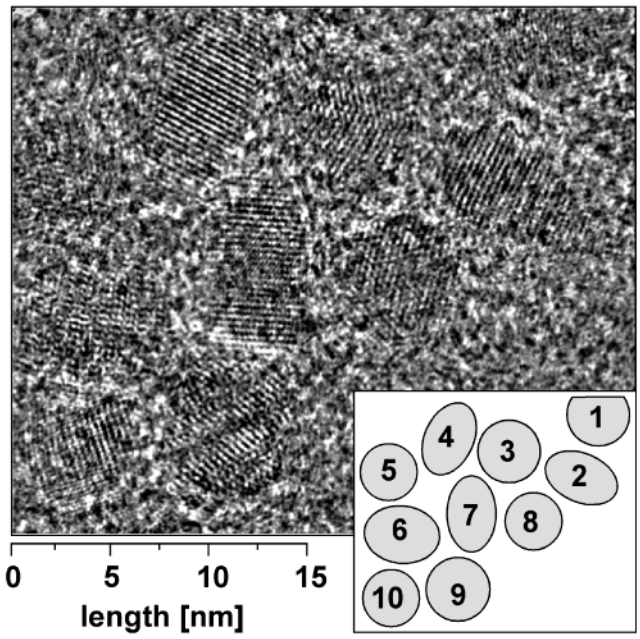


**Figure 3.** High-resolution TEM image of several CdSe/ZnS nanoparticles on an amorphous carbon support. Only a third of all of the particles are single-domain crystallites. The remaining nanocrystals show stacking faults of different degrees or are even polycrystalline. The numbers in the inset are used to label the different particles for discussion in the text.

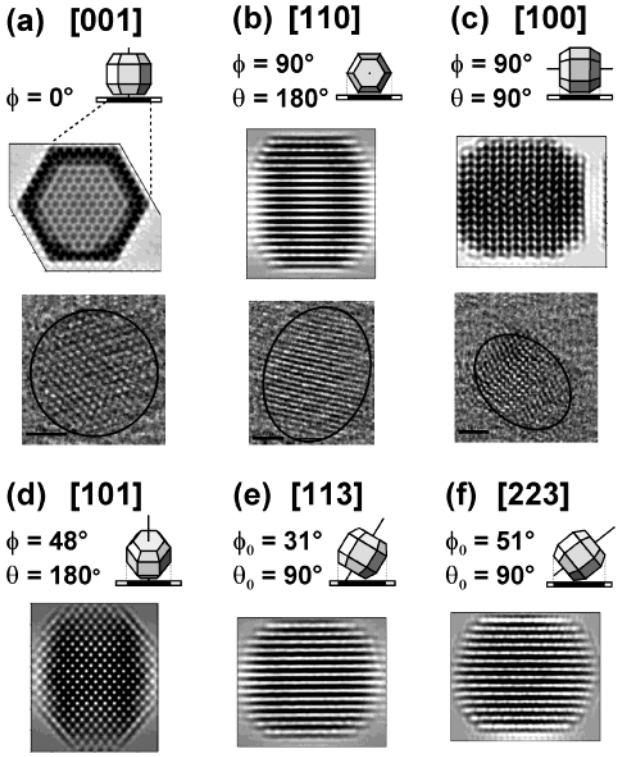


**Figure 4.** TEM image simulation of CdSe nanocrystals that are aligned along specific crystallographic orientations. All images are calculated for the Scherzer focus. In addition, three experimental TEM images are shown. (For details, see text.)

several hours, resulting in a thermodynamically stable, almost spherical particle shape.[54] In contrast, a high precursor concentration leads to the formation of strongly elongated nanorods.[54−57] The crystallinity of the nanocrystals is quite diverse, exhibiting many different patterns of regular and irregular lattice fringes. In the following discussion, we will distinguish between three kinds of particles: If particles show regular lattice fringes, we assume that these are ideal nanocrystals from which the crystallographic orientation with respect to the substrate could be determined, in principle. Possible candidates are particle nos. 2 and 4 with parallel lattic fringes and also particle no. 8, where the TEM image is consistent with the view along the crystallographic [001] axis, as has already been described.[22] The second class of particles are those that show stacking faults, such as particle nos. 3 and 9. The third class is polycrystalline particles where only small sections of the lattice fringes can be resolved in the TEM images. For example, particle nos. 1 and 5 would belong to this class of nanocrystals. From the investigation of several HRTEM images containing a total of 80 different particles, we found that 30% can be attributed to ideal nanocrystals whereas 25% showed stacking faults, and the remaining 45% belong to the polycrystalline variety.

The simulation of the HRTEM images for ideal CdSe nanocrystals with different orientations was performed at Scherzer focus using the HRTEM module of the software package Cerius$^2$.[58] The constructed model of the CdSe particle with bulk hcp crystal structure ($a = b = 0.43$ nm and $c = 0.7$ nm, space group $P63mc$) contains $14 \times 14 \times 9$ unit cells leading to a hexagonal prismatic crystallite with an extension of approximately 6.3 nm in the [001] direction and an aspect ratio of 1.3.[22] For the simulations, the crystal is placed into a box with 20-nm cell dimensions. The six projections that are expected to give rise to the clearest high-resolution images are shown in Figure 4 together with a schematic drawing of the crystal tilt. In Figure 4a, the particle is aligned along the $c$ axis [001] of the hexagonal structure, and the crossed [100] lattice planes ($d = 0.37$ nm) are exposed. As an example, an experimental image of one particular NC from the investigated sample with the same assumed orientation on the substrate and perfect crystallinity is shown below. The simulated images in Figure 4b and c resemble a 90° tilt over a side and an edge of the particle, leading to views down the [100] and [110] axes, respectively. The experimental high-resolution images below show experimental HRTEM images of nanocrystals from the investigated sample, which resemble the simulated images. The simulated HRTEM images in the lower row show projections along the crystallographic [101], [113], and [223] axes for d, e, and f, respectively. It is noted that the projections that result in parallel lines e and f show line spacings of 0.37 nm. Because this is close to the simulated line distances of the particle shown in Figure 4b (0.35 nm), we assume that these orientations cannot be distinguished properly in the experimental images.

## IV. Optical Investigation

The comparison of the crystallinity or even the crystal orientation of single nanocrystals with their fluorescence characteristics is possible only for particles that are deposited in low concentration on a substrate with markers as described above. In general, the optical investigations were always performed first because no fluorescence light could be detected from particles after the TEM measurements.[59]

To obtain HRTEM images with a high contrast, the particles were deposited directly on the $Si_3N_4$ substrates without an embedding matrix. Such particles are directly exposed to the gas environment,[60] which leads to strong fluorescence fluctuations[30] and fast photocorrosion.[31] As a consequence, the fluorescence could sometimes be observed for just a few seconds, even though the measurements were performed under a continuous

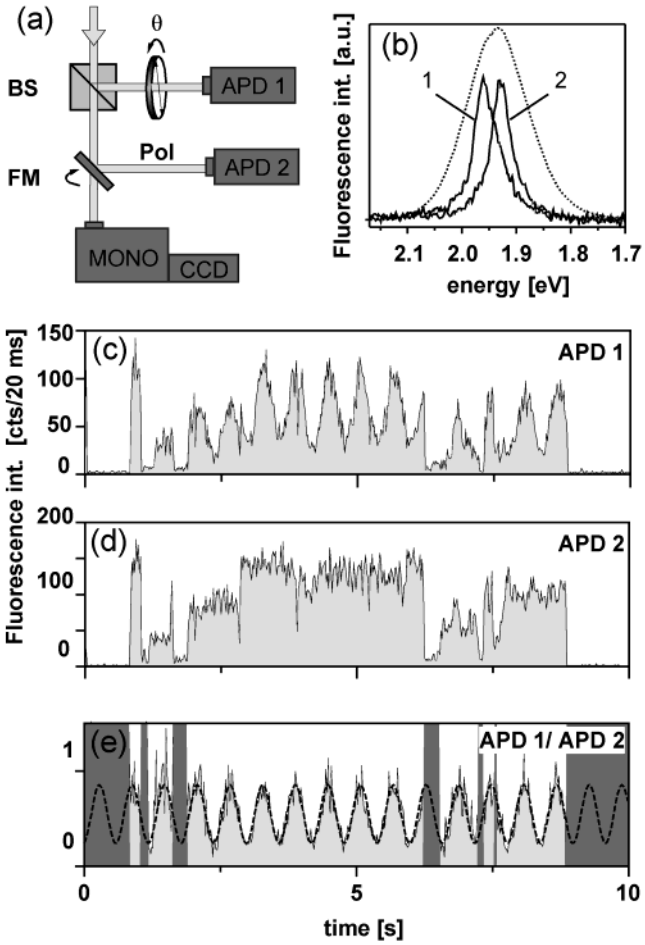


**Figure 5.** Detection scheme and typical fluorescence transients used to determine the fluorescence polarization. (a) The fluorescence light is divided by a beam splitter (BS) and guided to two detectors (APD1 and 2) simultaneously, and a rotating polarizer (POL) is placed in front of APD1. Fluorescence spectra can be taken by moving the flip mirror (FM). (b) Fluorescence spectra of the nanocrystal ensemble (dotted line) and of two individual particles (1 and 2). (c) Fluorescence transient at APD1 behind the rotating polarizer and (d) APD2 without the polarizer. (e) Ratio of APD1 (c) and APD2 (d), which shows only the polarization modulation and can be fitted with a single $\cos^2$ function.

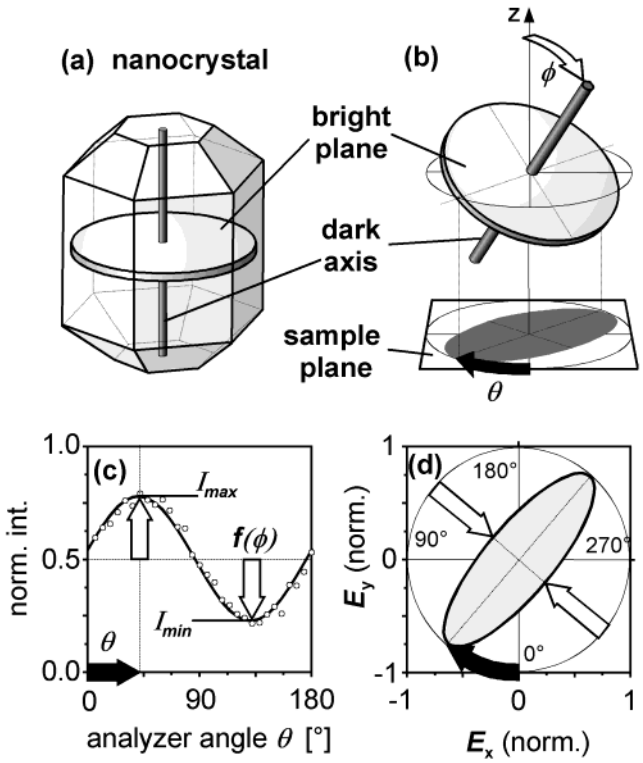


**Figure 6.** Analysis of the fluorescence polarization modulation for a hexagonal CdSe nanocrystal as suggested by ref 42. (a) A hexagonal 3D CdSe nanocrystal has a 2D transition dipole (bright plane) and perpendicular to this plane a 1D dark axis. (b) Because the nanocrystal can be arbitrarily tilted, the projection of the bright plane onto the sample plane appears as an ellipsoid, where the ellipticity depends on the tilt angle ($\phi$). (c) A rotating polarizer in the observation plane results in an intensity modulation that can be fitted with a function where the modulation depth ($I_{min} - I_{max}$) depends on the tilt angle ($\phi$) and the phase of the in-plane angle ($\Theta$). (Experimental data is taken from Figure 5.) (d) Polarization ellipsoid as calculated from the fit function drawn in c.

argon flow. Therefore, we developed a technique that corrects for the blinking effect and allows us to determined the degree of fluorescence polarization within seconds by using two detectors simultaneously (Experimental Section).

A fluorescence spectrum of an ensemble of nanocrystals (dotted line) and two spectra of individual emitters 1 and 2 are shown in Figure 5b. To measure the fluorescence anisotropy of emitter 1, the fluorescence light is split and guided simultaneously to APD1 and APD2. The transient signal behind the rotating polarizer (Figure 5c) shows a periodic modulation due to the anisotropic polarization of the fluorescence light, which is superimposed on the intensity fluctuations due to the random blinking behavior. Because APD2 records the intensity fluctuations only (Figure 5d), the ratio of APD1/APD2 in Figure 5e reflects the pure polarization modulation. Here it can clearly be seen that neither the phase nor the modulation depth changes during the investigation (i.e, there seems to be no correlation between the intensity fluctuations and the fluorescence polarization). Therefore, complete information about the polarization modulation can be extracted, even if the fluorescence intensity is strongly fluctuating.

Besides the investigation of the polarization state, this experimental setup also allows us to distinguish between the fluorescence of a single emitter or a small aggregate of randomly aligned nanocrystals. If several particles contribute to the fluorescence signal, then the different particles would most likely be randomly aligned. The additional arbitrary intensity fluctuation of the different particles would then lead to a change in the phase and modulation depth of the normalized transient during the investigation. In fact, we have observed several luminescing spots that showed this behavior. Here we concentrate on results only where the normalized fluorescence intensity modulation can be fitted with a single $\cos^2$ function of angle $\theta$, as shown by the dotted line in Figure 5e.

The analysis of the fluorescence polarization data is based on previous work of Empedocles et al., who investigated the fluorescence polarization of individual CdSe/ZnS particles at low temperature, where the blinking frequency is strongly reduced.[42] They showed that the data can be analyzed by the assumption that individual nanocrystals have a 2D fluorescence transition dipole, a so-called bright plane (Figure 6a). In contrast, most organic dye molecules have a 1D transition dipole, a bright axis.[61]

In general, the intensity modulation of the fluorescence light caused by the rotating polarizer is due to the projection of the transition dipole onto the substrate plane. Therefore, the fluorescence intensity of a chromophore with a bright axis is zero if the projection of the transition dipole is perpendicular to the polarizer axis.[61] In contrast, Empedocles et al. found that the polarization modulation of nanocrystals has a finite depth

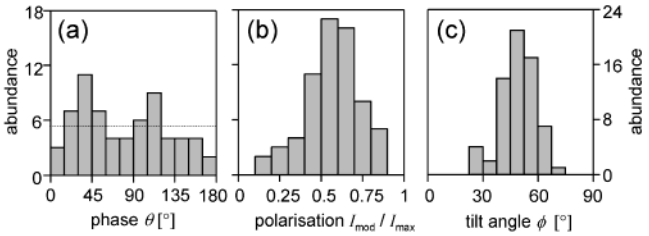


**Figure 7.** Statistics of the phase and tilt angles (Θ and $\phi$) for 65 individual nanocrystals. The in-plane angle (Θ) is randomly distributed within the experimental error. The maximum of the calculated tilt angle distribution is found at about $\phi = 50°$.

in most cases because the projection of a tilted bright plane onto the substrate is an ellipsoid (Figure 6b). Therefore, the 3D orientation of the bright plane can in principle be directly calculated form the degree of polarization. This information is determined by the tilt angle $\phi$ of the dark axis, which is perpendicular to the bright plane with respect to the observation direction: $\phi = 0°$ yields unpolarized fluorescence light ($I_{max} = I_{min}$) whereas $I_{min}$ is zero at $\phi = 90°$. As sketched in Figure 6b, $0° < \phi < 90°$ results in elliptically polarized light (Figure 6c and d). The phase $\theta$ of the detected modulation gives direct information about the orientation of the bright plane in the observation plane. Therefore, under the assumption that the bright plane lies in the crystallographic *a*,*b* plane,[62] the full 3D orientation of the nanocrystals could be gained from the fluorescence polarization measurements, in principle.

We have used this model to analyze the polarization behavior of 65 individual emitters. Figure 7a shows the distribution of the modulation phases $\theta$, which is a direct measure of the bright plane orientation. It can be seen that the phases are randomly distributed within the experimental error. Figure 7b and c shows the distribution of the polarization degree $V = (I_{max} - I_{min})/(I_{max})$ and the tilt angles $\phi$ as calculated according to $I_{min}/I_{max} = \cos^2 \phi$. The statistics of the polarization behavior is in good agreement with the data taken by Empedocles et al. at low temperature.[42] Therefore, we assume that the optical quality of our sample is similar to that of the previously investigated nanocrystals and that the results can be directly compared with each other.

It should be mentioned at this point that there is some uncertainty about the distribution of the out-of-plane angle $\phi$ of the 2D transition dipole. First, the radiation characteristics of the nanocrystals might be influenced by the air/$Si_3N_4$ interface because the particles are deposited directly on the substrate. Also, the collection angle of the microscope objective needs to be taken into account, as has been discussed in detail elsewhere.[42] However, experiments with chromophores exhibiting a 1D bright plane, which have been performed with the same experimental setup for comparison, revealed that the error is only on the order of 10%.

## V. Combined Optical and Structural Investigation

The investigation of the same particles in a TEM after the optical investigations turned out to be quite demanding from an experimental point of view. First, because of the small diameter of the nanocrystals, they can be localized in the TEM only at high magnification (>20−30k). At the same time, it is necessary to image a specific marker element together with the nanocrystals to determine the exact position of the particles. Therefore, only those nanocrystals that were spatially closer than about 1 $\mu$m from a prominent electrode structure could be investigated. Second, in most cases, more than one particle could

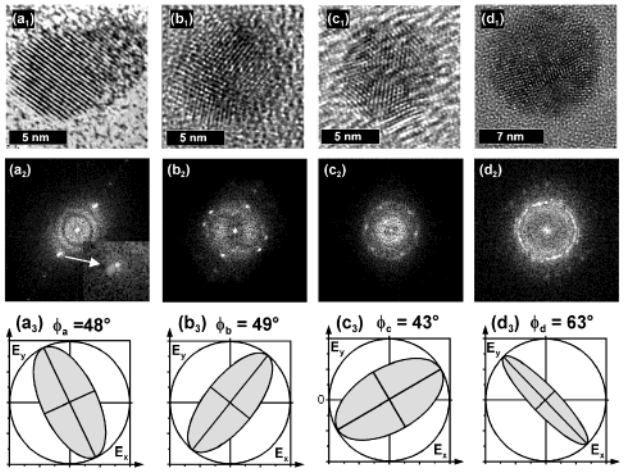


**Figure 8.** High-resolution TEM images (index 1), Fourier transform (FT) of the images (index 2), and fluorescence polarization ellipsoids (index 3) of four individual nanocrystals (a−d), which could be localized and investigated by TEM and fluorescence microscopy. All particles are almost spherical but show elliptically polarized fluorescence. Particle a is a single-domain crystal where the shadow on the upper right side might result from ZnS. The inset in the FT shows a blurry reflex at higher momentum corresponding to a lower lattice constant of ZnS. The orientation of this particular particle might have changed during the TEM investigation. Particles b and c show several stacking faults corresponding to multiple pairs of reflexes in the FTs and emit ellipsoidal polarized light. Particle d is even polycrystalline, resulting in a diffuse ring in the FT, and shows the strongest polarization anisotropy.

be localized by TEM in the area of a diffraction-limited luminescing spot. Obviously, only a fraction of the particles deposited on the surface gave rise to luminescence.[59] This is consistent with measurements of combined AFM and optical experiments that showed that a luminescence signal could be detected only from 30 to 50% of the nanocrystals.[63] However, a direct correlation between the structure and the fluorescence polarization cannot be performed under such circumstances because it is not known which particle has been optically investigated before. Last but not least, the $Si_3N_4$ membranes turned out to be very fragile. From the four substrates that we had at our disposal, two broke during sample transfer, and one was destroyed during the high-resolution TEM investigations. Therefore, out of 65 nanocrystals, which were investigated in detail optically, only 4 nanocrystals could be unambiguously assigned in the corresponding HRTEM image.

The HRTEM pictures and fluorescence polarization data for these four particles are summarized in Figure 8. The first row shows the HRTEM pictures (index 1), and the second row, the resulting Fourier transforms (FT) of these images (index 2), which directly reflect the diffraction patterns of the particles. The third row (index 3) comprises the corresponding polarization ellipsoids that were determined according to the procedure depicted in Figure 6.

First, it can be seen that the four particles are almost spherical in shape and show different degrees of lattice imperfections. In the context of the classification established in Figure 3, we assume that particle a is an ideal particle whereas particles b and c fall into the stacking faults category and particle c is polycrystalline.

The parallel lattice fringes of the TEM image in $a_1$ result in only one set of calculated diffraction peaks in the FT image shown in $b_1$. The shadow in the upper right part of $a_1$ might result from imperfectly grown ZnS onto the CdSe particle. This

is supported by the fact that the calculated FT of the TEM picture (inset in $a_2$) reveals two close-lying spots that would correspond to the (100) lattice constants of CdSe (0.37 nm) and ZnS (0.33 nm). The fluorescence polarization data of this particle could be fitted with a fluorescence anisotropy of $V = 0.39$, resulting in the shape of the corresponding ellipsoid as shown in Figure 8 ($a_3$). The values of orientation angles $\phi$ and $\theta$ (Figure 6) as calculated from the fluorescence measurements are $\phi = 48°$ and $\theta = -25°$ respectively. However, there is some uncertainty about the orientation of this particular particle: in contrast to particles b, c, and d, particle a was buried in some residue of unknown composition, possibly an excess of the ligands, and the HRTEM image could be taken only after the matrix was evaporated with the electron beam of the electron microscope. Therefore, the orientation of this particle might have changed during the matrix desorption process in the HRTEM. Hence, the direction of the polarization ellipsoid might not be directly comparable with the crystallographic orientation of this particular particle.

In contrast, particles b, c, and d were found without any residues, and no change in the HRTEM pictures was observed in consecutive images. Particle b could even be found with two different electron microscopes, yielding comparable HRTEM images. Therefore, the optical and TEM data of particles b, c, and d can be directly compared with each other.

According to the HRTEM images, the diameters of particles b and c were determined to be 9 and 8.5 nm, respectively. These nanocrystals show several crossings of lattice fringes that result in the calculated diffraction pattern shown in the Figures ($b_2$ and $c_2$). A simulation of TEM images from CdSe nanocrystals with an ideal *hcp* lattice structure using different shapes and orientations did not lead to any correspondence with the observed high-resolution images. Therefore, we assume that the formation of stacking faults during particle growth or the nonepitaxial growth of the ZnS shell is responsible for the complex lattice structures of b and c. Comparable images have been found for Ag and Au nanoparticles, for example.[64,65]

Particle b exhibits mainly two domains grown together under approximately 90°, which is possible for the [100] or [110] direction. The smaller lattice-plane distances in the lower right part could again be assigned to the ZnS material. To explain the image of particle c, at least three individual domains that are grown together under an angle of 60° need to be taken into account. Comparing with the simulations suggests the crystallographic domains to be [001] or [101]. Lattice spacings resulting from nonepitaxially grown ZnS material could not be observed for this particle. By comparing the polarization ellipsoids ($b_3$, $V = 0.41$ and $c_3$, $V = 0.30$) with the corresponding diffraction patterns ($b_2$ and $c_2$, respectively), we note that the elongation direction of the ellipsoids is aligned along one set of diffraction patterns (i.e., perpendicular to the corresponding lattice planes). Under the assumption that these are the lattice planes of the CdSe core, this could be the first indication that the bright plane indeed lies perpendicular to the crystallographic *c* axis.

The HRTEM image ($d_1$) indicates a relatively large particle with a diameter of about 12 nm. From this particular particle, we were also able to record a fluorescence spectrum (not shown) that had a fluorescence maximum at 630 nm corresponding to a CdSe core diameter of only about 6 nm. Therefore, we assume that this particle has a particularly thick ZnS shell that obviously grew in a nonepitaxial manner around the CdSe nanocrystal. This is illustrated by the diffuse diffraction ring in the FT image ($d_2$). However, a closer look at Figure 8 ($d_2$) reveals that at least three sets of second-order peaks can be seen in the FT and that the fluorescence polarization ellipsoid is elongated in this direction, which is similar to that for particles b and c. The degree of fluorescence polarization for particle d was determined to be as high as $V = 0.65$.

## VI. Discussion

There is a long-standing debate as to which extended fluorescence properties of semiconductor nanocrystals are governed by surface effects or by the crystal structure (see, for example, ref 2). In the following discussion, we will examine our experimental results as to what extent they allow us to distinguish between these two effects.

Starting with the CdSe core, we note that the fluorescence quantum yield is relatively small (<1%). This is in agreement with a recent study by Peng et al., who investigated the fluorescence yield of CdSe particles as a function of reaction time, precursor concentrations, and surface ligands.[51,66] The authors demonstrated that the fluorescence yield is strongly dependent on the surface properties of the particles (i.e., on the composition of the outermost inorganic shell and also the passivating surface ligands). They defined a so-called "bright point" at which the fluorescence yield reaches a maximum, which decreases upon further crystal growth. It is reasonable to assume that the low fluorescence quantum yield of our core particles results from the long reaction time, which was needed to prepare large particles to be easily found in the TEM experiments. However, we could show that the fluorescence yield is strongly increased by covering these CdSe cores with a few monolayers of ZnS in a mixture of TOPO and DA as the solvent. Because the high fluorescence quantum yield can therefore be obtained by the surface modification of CdSe cores with an initially low quantum yield, this is the first indication that the surface structure rather than the crystallinity is responsible for the fluorescence quantum yield.

Another argument for this assumption comes from the fact that no fluorescence could be observed for particles that have been investigated by TEM before. Most likely, the irradiation with high-energy electrons leads to a desorption of the molecular ligands and therefore to unsaturated inorganic sites at the particles' surface, which might act as traps for the photogenerated electrons and/or holes. It should be mentioned at this point that we also observed a change in particle crystallinity during TEM investigations in some cases. For example, if a polycrystalline particle is exposed to the focused electron beam for a longer time (several tens of seconds), then we could observe a recrystallization up to the point where an ideal crystal structure such as that presented in the simulations could be found.[67]

Finally, the reversible change in fluorescence yield upon exposure to different gases further supports the model.[30] When single CdSe/ZnS particles are exposed to oxygen instead of argon, the nanocrystals stay in the nonfluorescing "off" state much longer. Because the particles investigated in this work were directly exposed to the ambient gas environment, the fluorescence intensity fluctuations were very strong. Interestingly, we could clearly show that the fluorescence fluctuations are not correlated to the fluorescence polarization. The results of our fluorescence polarization study of 65 individual particles are in agreement with the measurements of Empedocles et al., which have been performed at cryogenic temperature.[42] In this work, it has already been argued that the orientation of the fluorescence transition dipole does not depend on surface effects but rather is related to the crystal structure, shape, or orientation of the particles.

The TEM investigation showed that only 30% of the particles are single-domain crystals and that the rest shows stacking faults of different degrees or are even polycrystalline. However, crystallographic investigations of CdSe particles without a ZnS shell have shown that on average only one stacking fault per nanocrystal is found.[3,22] The discrepancy can again be explained by the different growth conditions. While the growth time for the relatively small CdSe particles was just a few minutes,[22] the nanocrystals investigated in the present work were grown over several hours. Because of the long reaction time, the growth takes place in the so-called Ostwald ripening regime, where small particles dissolve and grow onto the larger particles.[48,68] This slow growth mode might result in an increased number of lattice imperfections. Additionally, the coverage with ZnS often is not strictly epitaxially and can lead to additional stacking faults.[47]

The TEM localization of single particles, which have been investigated by fluorescence measurements before, turned out to be very difficult. Because a particle has to be within 1 $\mu$m of a specific marker, most of the nanocrystals found in the fluorescence images cannot be traced back in the TEM pictures. Further studies should be performed on substrates with a more regular pattern, with marker distances in the range of 1 $\mu$m.

Despite these complications, the four particles that could be localized in the optical and TEM experiments already allow us to draw conclusions about the correlation between the structural and optical properties. First, although they show very different crystallinity ranging from a single-domain crystal to more or less polycrystalline materials, all nanocrystals gave rise to a fluorescence signal strong enough for single-particle studies. This is the strongest argument that the crystallinity has only a minor effect on the fluorescence yield. Second, all of the particles are nearly spherical but show ellipsoidal polarized fluorescence light. The polarization modulation was strongest for the largest particle, which, at the same time, is the nanocrystal with the highest degree of lattice imperfections. However, because the few successful measurements have no statistical relevance, it has not been worth arguing if the size, the orientation, or the lack of crystallinity is the reason for the high degree of polarization anisotropy.

A strict correlation of the crystallographic orientation on the substrate with the orientation of the transition dipole can presently not be performed with the data at hand. Even if only single-domain particles could be found in the TEM, this would be very difficult because there are many different crystallographic orientations that give rise to parallel lattice fringes. Therefore, the specific crystallographic orientation can be determined directly only in a very few cases, such as that for the [100] or [001] alignment. Another possibility would be a series of TEM images with increasing tilt of the nanocrystal until a distinct crystallographic orientation can be seen, from which the original orientation can be deduced.[67]

## Summary

In summary we have performed fluorescence measurements of single CdSe/ZnS nanocrystals and a detailed complementary TEM investigation. The results show that the fluorescence yield and intensity fluctuations are not dependent on the crystallinity. We demonstrated that the degree and orientation of the fluorescence polarization can be determined by a method that uses a second detector to account for intensity fluctuations. The results of the polarization measurements show that spherical particles emit ellipsoidal polarized light, even at room temperature. A comparison of the optical measurements with TEM results further indicates that even polycrystalline particles may emit elliptically polarized light. Therefore, it is not straightforward to determine the 3D crystallographic orientation of the nanocrystal with respect to the substrate solely from fluorescence measurements of single nanocrystals.

**Acknowledgment.** This work was supported by the DFG under contract no. ME 1380/6-1.

## References and Notes

(1) Alivisatos, A. P. *J. Phys. Chem.* **1996**, *100*, 13226.
(2) Yoffe, A. D. *Adv. Phys.* **2001**, *50*, 1.
(3) Murray, C. B.; Norris, D. J.; Bawendi, M. G. *J. Am. Chem. Soc.* **1993**, *115*, 8706.
(4) Kuno, M.; Lee, J. K.; Dabbousi, B. O.; Mikulec, F. V.; Bawendi, M. G. *J. Chem. Phys.* **1996**, *106*, 9869.
(5) Schmelz, O.; Mews, A.; Basché, T. *Langmuir* **2001**, *17*, 2861.
(6) Spanhel, L.; Haase, M.; Weller, H.; Henglein, A. *J. Am. Chem. Soc.* **1987**, *109*, 5649.
(7) Kortan, A. R.; Hull, R.; Opila, R. L.; Bawendi, M. G.; Steigerwald, M. L.; Caroll, R. J.; Brus, L. E. *J. Am. Chem. Soc.* **1990**, *112*, 1327.
(8) Hässelbarth, A.; Eychmüller, A.; Eichberger, R.; Giersig, M.; Mews, A.; Weller, H. *J. Phys. Chem.* **1993**, *97*, 5333.
(9) Mews, A.; Eychmüller, A.; Giersig, M.; Schooss, D.; Weller, H. *J. Phys. Chem.* **1994**, *98*, 934.
(10) Peng, X.; Schlamp, M. C.; Kadavanich, A. V.; Alivisatos, A. P. *J. Am. Chem. Soc.* **1997**, *119*, 7019.
(11) Hines, M. A.; Guyot-Sionnest, P. *J. Phys. Chem.* **1996**, *100*, 468.
(12) Colvin, V. L.; Schlamp, M. C.; Alivisatos, A. P. *Nature* **1994**, *370*, 354.
(13) Dabbousi, B. O.; Bawendi, M. G.; Onitzuka, O.; Rubner, M. F. *Appl. Phys. Lett.* **1995**, *66*, 1316.
(14) Schlamp, M. C.; Peng, X. G.; Alivisatos, A. P. *J. Appl. Phys.* **1997**, *82*, 5837.
(15) Lee, J.; Sundar, V. C.; Heine, J. R.; Bawendi, M. G.; Jensen, K. F. *Adv. Mater.* **2000**, *12*, 1102.
(16) Bruchez, M.; Moronne, M.; Gin, P.; Weiss, S.; Alivisatos, A. P. *Science* **1998**, *281*, 2013.
(17) Chan, W. C. W.; Nie, S. *Science* **1998**, *281*, 2016.
(18) Klimov, V. I.; Mikhailovsky, A. A.; Xu, S.; Malko, A.; Hollingsworth, J. A.; Leatherdale, C. A.; Eisler, H. J.; Bawendi, M. G. *Science* **2000**, *290*, 314.
(19) Kazes, M.; Lewis, D. Y.; Ebstein, Y.; Mokari, T.; Banin, U. *Adv. Mater.* **2002**, *14*, 317.
(20) Norris, D. J.; Bawendi, M. G. *Phys. Rev. B* **1996**, *53*, 16338.
(21) Mews, A.; Eychmüller, A. *Ber. Bunsen-Ges. Phys. Chem.* **1998**, *102*, 1343.
(22) Shiang, J. J.; Kadavanich, A. V.; Grubbs, R. K.; Alivisatos, A. P. *J. Phys. Chem.* **1995**, *99*, 17417.
(23) Mews, A.; Kadavanich, A. V.; Banin, U.; Alivisatos, A. P. *Phys. Rev. B* **1996**, *53*, R13242.
(24) Kadavanich, A. V.; Kippeny, T. C.; Erwin, M. M.; Rosenthal, S. J. *J. Phys. Chem. B* **2001**, *105*, 361.
(25) Klein, D. L.; Roth, R.; Lim, A. K. L.; Alivisatos, A. P.; McEuen, P. L. *Nature* **1997**, *389*, 699.
(26) Banin, U.; Katz, Y. W.; Millo, O. *Nature* **1999**, *400*, 542.
(27) Empedocles, S. A.; Neuhauser, R.; Shimizu, K.; Bawendi, M. G. *Adv. Mater.* **1999**, *11*, 1243.
(28) Nirmal, M.; Dabbousi, B. O.; Bawendi, M. G.; Macklin, J. J.; Trautman, J. K.; Harris, T. D.; Brus, L. E. *Nature* **1996**, *383*, 802.
(29) Tittel, J.; Ghde, W.; Koberling, F.; Basché, T.; Kornowski, A.; Weller, H.; Eychmüller, A. *J. Phys. Chem. B* **1997**, *101*, 3013.
(30) Koberling, F.; Mews, A.; Basché, T. *Adv. Mater.* **2001**, *13*, 672.
(31) van Sark, W. G. J. H. M.; Frederix, P. L. T. M.; Bol, A. A.; Gerritsen, H. C.; Meijerink, A. *ChemPhysChem.* **2002**, *3*, 871.
(32) Banin, U.; Bruchez, M.; Alivisatos, A. P.; Ha, T.; Weiss, S.; Chemla, D. S. *J. Chem. Phys.* **1999**, *110*, 1195.
(33) Verberk, R.; van Oijen, A. M.; Orrit, M. *Phys. Rev. B* **2002**, *66*, 233202.
(34) Neuhauser, R. G.; Shimizu, K. T.; Woo, W. K.; Empedocles, S. A.; Bawendi, M. G. *Phys. Rev. Lett.* **2000**, *85*, 3301.
(35) Chepic, D. I.; Efros, A. L.; Ekimov, A. I.; Ivanov, M. G.; Kharchenko, V. A.; Kudriavtsev, I. A.; Yazeva, T. V. *J. Lumin.* **1990**, *47*, 113.
(36) Krauss, T. D.; Brus, L. *Phys. Rev. Lett.* **1999**, *83*, 4840.
(37) Kapitonov, A. M.; Stupak, A. P.; Gaponenko, S. V.; Petrov, E. P.; Rogach, A. L.; Eychmueller, A. B. *J. Phys. Chem. B* **1999**, *103*, 10109.
(38) Michler, P.; Imamoglu, A.; Mason, M. D.; Carson, P. J.; Strouse, G. F.; Buratto, S. K. *Nature* **2000**, *406*, 968.
(39) Lounis, B.; Bechtel, H. A.; Gerion, D.; Alivisatos, P.; Moerner, W. E. *Chem. Phys. Lett.* **2000**, *329*, 399.

(40) Schlegel, G.; Bohnenberger, J.; Potapova, I.; Mews, A. *Phys. Rev. Lett.* **2002**, *88*, 137401.
(41) Shimizu, K. T.; Woo, W. K.; Fisher, B. R.; Eisler, H. J.; Bawendi, M. G. *Phys. Rev. Lett.* **2002**, *89*, 117401,1.
(42) Empedocles, S. A.; Neuhauser, R.; Bawendi, M. G. *Nature* **1999**, *399*, 126.
(43) Efros, A. L.; Rodina, A. V. *Phys. Rev. B* **1993**, *47*, 10005.
(44) Hu, J.; Li, L.; Yang, W.; Manna, L.; Wang, L.; Alivisatos, A. P. *Science* **2001**, *292*, 2060.
(45) Hu, J.; Wang, L.; Li, L.; Yang, W.; Alivisatos, A. P. *J. Phys. Chem.* **2002**, *106*, 2447.
(46) Wang, X.-Y.; Zhang, J.-Y.; Nazzal, A.; Darragh, M.; Xiao, M. *Appl. Phys. Lett.* **2002**, *81*, 4829.
(47) Dabbousi, B. O.; Rodriguez-Viejo, J.; Mikulec, F. V.; Heine, J. R.; Mattoussi, H.; Ober, R.; Jensen, K. F.; Bawendi, M. G. *J. Phys. Chem. B* **1997**, *101*, 9463.
(48) Peng, X.; Wickham, J.; Alivisatos, A. P. *J. Am. Chem. Soc.* **1998**, *120*, 5343.
(49) Talapin, D. V.; Rogach, A. L.; Kornowski, A.; Haase, M.; Weller, H. *Nano Lett.* **2001**, *1*, 207.
(50) Wu, S. Y.; Casida, J. E. *PSSLEC* **1995**, *102*, 177.
(51) Qu, L.; Peng, X. *J. Am. Chem. Soc.* **2002**, *124*, 2049.
(52) Philipp, G.; Weimann, T.; Hinze, P.; Burghard, M.; Weis, J. *Microelectron. Eng.* **1999**, *46*, 157.
(53) Mews, A.; Koberling, F.; Basché, Philipp, G.; Duesberg, G.; Roth, S.; Burghard, M. *Adv. Mater.* **2000**, *12*, 1210.
(54) Peng, Z. A.; Peng, X. *J. Am. Chem. Soc.* **2002**, *124*, 3343.
(55) Peng, X.; Manna, L.; Yang, W.; Wickham, J.; Scher, E.; Kadavanich, A.; Alivisatos, A. P. *Nature* **2000**, *404*, 59.
(56) Manna, L.; Scher, E. C.; Alivisatos, A. P. *J. Am. Chem. Soc.* **2000**, *122*, 12700.
(57) Peng, Z. A.; Peng, X. *J. Am. Chem. Soc.* **2001**, *123*, 1389.
(58) *Cerius*$^2$, version 4.2MS (molecular modeling environment); Accelrys Inc.: San Diego, CA.
(59) Koberling, F.; Mews, A.; Philipp, G.; Kolb, U.; Potapova, I.; Burghard, M.; Basché, T. *Appl. Phys. Lett.* **2002**, *81*, 1116.
(60) Koberling, F.; Mews, A.; Potapova, I.; Basché, T. *Proc. SPIE* **2001**, *4456*, 31.
(61) Ha, T.; Laurence, T. A.; Chemla, D. S.; Weiss, S. *J. Phys. Chem. B* **1999**, *103*, 6839.
(62) Efros, A. L. *Phys. Rev. B* **1992**, *46*, 7448.
(63) Ebstein, Y.; Mokari, T.; Banin, U. *Appl. Phys. Lett.* **2002**, *80*, 4033.
(64) Hofmeister, H.; Claus, P. *10th Annual Meeting of DGK*; Kiel, Germany, 2002.
(65) Ascencio, J. A.; Gutierrez-Wing, C.; Espinosa, M. E.; Marin, M.; Tehuacanero, S.; Zorilla, C.; Jose-Yacaman, M. *Surf. Sci.* **1988**, *396*, 349.
(66) Zhang, J.; Wang, X. Y.; Xiao, M.; Qu, L.; Peng, X. *Appl. Phys. Lett.* **2002**, *81*, 2076.
(67) Kolb, U. To be submitted for publication.
(68) Talapin, D. V.; Rogach, A. L.; Haase, M.; Weller, H. *J. Phys. Chem. B* **2001**, *105*, 12278.